High bandwidth on-chip silicon photonic interleaver

Lian-Wee Luo,[1] Salah Ibrahim,[2] Arthur Nitkowski,[1] Zhi Ding,[2] Carl B. Poitras, [1] S. J. Ben Yoo,[2] and Michal Lipson[1,3,*]

[1]*School of Electrical and Computer Engineering, Cornell University, Ithaca, New York 14853, USA*
[2]*Department of Electrical and Computer Engineering, University of California, Davis, California 95616, USA*
[3]*Kavli Institute at Cornell for Nanoscale Science, Cornell University, Ithaca, New York 14853, USA*
**ml292@cornell.edu*

Abstract: We demonstrate a 120 GHz 3-dB bandwidth on-chip silicon photonic interleaver with a flat passband over a broad spectral range of 70 nm. The structure of the interleaver is based on an asymmetric Mach-Zehnder interferometer (MZI) with 3 ring resonators coupled to the arms of the MZI. The transmission spectra of this device depict a rapid roll-off on the band edges, where the 20-dB bandwidth is measured to be 142 GHz. This device is optimized for operation in the C-band with a channel crosstalk as low as –20 dB. The device also has full reconfiguration capability to compensate for fabrication imperfections.

OCIS codes: (130.3120) Integrated optics devices; (130.7408) Wavelength filtering devices; (250.5300) Photonic integrated circuits.

References and links

1. G. P. Agrawal, "Fiber-optic communication systems," 3rd ed. (Wiley, 2002).
2. M. Haurylau, G. Q. Chen, H. Chen, J. D. Zhang, N. A. Nelson, D. H. Albonesi, E. G. Friedman, and P. M. Fauchet, "On-chip optical interconnect roadmap: challenges and critical directions," IEEE J. Sel. Top. Quantum Electron. **12**(6), 1699–1705 (2006).
3. A. S. Liu, R. Jones, L. Liao, D. Samara-Rubio, D. Rubin, O. Cohen, R. Nicolaescu, and M. Paniccia, "A high-speed silicon optical modulator based on a metal-oxide-semiconductor capacitor," Nature **427**(6975), 615–618 (2004).
4. S. Manipatruni, Q. Xu, B. Schmidt, J. Shakya, and M. Lipson, "High speed carrier injection 18 Gb/s silicon micro-ring electro-optic modulator," in *The 20th Annual Meeting of the IEEE Lasers and Electro-Optics Society (IEEE, 2007)*, 537–538.
5. W. M. J. Green, M. J. Rooks, L. Sekaric, and Y. A. Vlasov, "Ultra-compact, low RF power, 10 Gb/s silicon Mach–Zehnder modulator," Opt. Express **15**(25), 17106–17113 (2007).
6. T. Yin, R. Cohen, M. M. Morse, G. Sarid, Y. Chetrit, D. Rubin, and M. J. Paniccia, "31 GHz Ge n-i-p waveguide photodetectors on silicon-on-insulator substrate," Opt. Express **15**(21), 13965–13971 (2007).
7. Y. M. Kang, H. D. Liu, M. Morse, M. J. Paniccia, M. Zadka, S. Litski, G. Sarid, A. Pauchard, Y. H. Kuo, H. W. Chen, W. S. Zaoui, J. E. Bowers, A. Beling, D. C. McIntosh, X. G. Zheng, and J. C. Campbell, "Monolithic germanium/silicon avalanche photodiodes with 340 GHz gain-bandwidth product," Nat. Photonics **3**(1), 59–63 (2009).
8. L. Chen, and M. Lipson, "Ultra-low capacitance and high speed germanium photodetectors on silicon," Opt. Express **17**(10), 7901–7906 (2009).
9. S. Assefa, F. N. A. Xia, and Y. A. Vlasov, "Reinventing germanium avalanche photodetector for nanophotonic on-chip optical interconnects," Nature **464**(7285), 80–84 (2010).
10. S. Cao, J. Chen, J. N. Damask, C. R. Doerr, L. Guiziou, G. Harvey, Y. Hibino, H. Li, S. Suzuki, K. Y. Wu, and P. Xie, "Interleaver technology: comparisons and applications requirements," J. Lightwave Technol. **22**(1), 281–289 (2004).
11. K. Jinguji, "Synthesis of coherent two-port optical delay-line circuit with ring waveguides," J. Lightwave Technol. **14**(8), 1882–1898 (1996).
12. K. Jinguji, and M. Oguma, "Optical half-band filters," J. Lightwave Technol. **18**(2), 252–259 (2000).
13. M. Oguma, T. Kitoh, Y. Inoue, T. Mizuno, T. Shibata, M. Kohtoku, and Y. Hibino, "Compact and low-loss interleave filter employing lattice-form structure and silica-based waveguide," J. Lightwave Technol. **22**(3), 895–902 (2004).
14. J. F. Song, Q. Fang, S. H. Tao, M. B. Yu, G. Q. Lo, and D. L. Kwong, "Passive ring-assisted Mach–Zehnder interleaver on silicon-on-insulator," Opt. Express **16**(12), 8359–8365 (2008).
15. J. F. Song, S. H. Tao, Q. Fang, T. Y. Liow, M. B. Yu, G. Q. Lo, and D. L. Kwong, "Thermo-optical enhanced silicon wire interleavers," IEEE Photon. Technol. Lett. **20**(24), 2165–2167 (2008).

16. J. F. Song, H. Zhao, Q. Fang, S. H. Tao, T. Y. Liow, M. B. Yu, G. Q. Lo, and D. L. Kwong, "Effective thermo-optical enhanced cross-ring resonator MZI interleavers on SOI," Opt. Express **16**(26), 21476–21482 (2008).
17. S. Darmawan, Y. M. Landobasa, P. Dumon, R. Baets, and M. K. Chin, "Nested-ring Mach–Zehnder interferometer in silicon-on-insulator," IEEE Photon. Technol. Lett. **20**(1), 9–11 (2008).
18. R. Essiambre, and P. J. Winzer, "Transport challenges in optically-routed networks," Proc. SPIE **6021**, 694–704 (2005).
19. JDSU Communications Components, "Bandsplitters 200 GHz Channel Spacing" (JDS Uniphase Corporation, 2010). *http://www.jdsu.com/product-literature/bandsplitter200_ds_cc_ae.pdf*.
20. K. Oda, N. Takato, H. Toba, and K. Nosu, "A wideband guided-wave periodic multi demultiplexer with a ring resonator for optical FDM transmission-systems," J. Lightwave Technol. **6**(6), 1016–1023 (1988).
21. C. K. Madsen, and J. H. Zhao, *Optical Filter Design and Analysis: A Signal Processing Approach* (Wiley, 1999).
22. Z. P. Wang, S. J. Chang, C. Y. Ni, and Y. J. Chen, "A high-performance ultracompact optical interleaver based on double-ring assisted Mach-Zehnder interferometer," IEEE Photon. Technol. Lett. **19**(14), 1072–1074 (2007).
23. A. Yariv, "Critical coupling and its control in optical waveguide-ring resonator systems," IEEE Photon. Technol. Lett. **14**(4), 483–485 (2002).
24. H. Takahashi, P. Carlsson, K. Nishimura, and M. Usami, "Analysis of negative group delay response of all-pass ring resonator with Mach–Zehnder interferometer," IEEE Photon. Technol. Lett. **16**(9), 2063–2065 (2004).
25. W. M. J. Green, R. K. Lee, G. A. Derose, A. Scherer, and A. Yariv, "Hybrid InGaAsP-InP Mach–Zehnder racetrack resonator for thermooptic switching and coupling control," Opt. Express **13**(5), 1651–1659 (2005).
26. W. D. Sacher, and J. K. S. Poon, "Characteristics of microring resonators with waveguide-resonator coupling modulation," J. Lightwave Technol. **27**(17), 3800–3811 (2009).
27. H. L. R. Lira, S. Manipatruni, and M. Lipson, "Broadband hitless silicon electro-optic switch for on-chip optical networks," Opt. Express **17**(25), 22271–22280 (2009).
28. N. Sherwood-Droz, H. Wang, L. Chen, B. G. Lee, A. Biberman, K. Bergman, and M. Lipson, "Optical 4x4 hitless slicon router for optical networks-on-chip (NoC)," Opt. Express **16**(20), 15915–15922 (2008).
29. K. Jinguji, N. Takato, A. Sugita, and M. Kawachi, "Mach–Zehnder interferometer type optical wave-guide coupler with wavelength-flattened coupling ratio," Electron. Lett. **26**(17), 1326–1327 (1990).
30. J. Van Campenhout, W. M. J. Green, S. Assefa, and Y. A. Vlasov, "Low-power, 2 x 2 silicon electro-optic switch with 110-nm bandwidth for broadband reconfigurable optical networks," Opt. Express **17**(26), 24020–24029 (2009).

1. Introduction

Optical interconnect networks utilizing wavelength-division multiplexing (WDM) technology present a solution to the electrical interconnect bottleneck by offering a larger bandwidth and lower power consumption in high-performance microelectronic chips [1,2]. To realize this goal, several high speed and low power silicon-based devices such as modulators and photodetectors have been reported [3–9]. High bandwidth interleavers are essential for routing a large number of WDM channels with high data-rate signals from one location to another location in a network [10]. A waveguide-based interleaver has been demonstrated using cascaded Mach-Zehnder interferometers (MZI), however this type of interleaver has a relatively large device footprint [11–13]. The number of cascaded MZI stages can be reduced and simplified by coupling ring resonators to the MZI. In ref [14–17]. silicon-based ring-assisted MZI interleavers have been designed and demonstrated, however their performance was limited in channel crosstalk and spectral range of operation due to the sensitivity of the device to fabrication imperfections.

Here we demonstrate a 120 GHz 3-dB bandwidth on-chip silicon photonic ring-assisted MZI interleaver that has a flat passband over a broad spectral range of 70 nm. This device is optimized to operate in the entire C-band with a channel crosstalk as low as −20 dB. The device also has full reconfiguration capability to compensate for fabrication imperfections.

2. Device design

We design an interleaver that has the capability of separating and combining a comb of WDM signals with low channel crosstalk and low signal distortion. The filtering function of such an interleaver is illustrated in Fig. 1(a). When a comb of WDM signals is coupled into the input of the interleaver, the device operates as a demultiplexer by channeling signals "1" to the bar port and signals "2" to the cross port. This device also operates as a multiplexer when signals (1' and 2') are coupled into the add port. Signal 1' is added to the signals at the cross port while signal 2' is added to the signals at the bar port. The transmission spectra of both the bar and cross ports in such an interleaver have a flat passband, a fast roll-off on the band edges, and a low channel crosstalk (i.e. high extinction ratio between the passband of one channel

and the stopband of an adjacent channel) [10]. Figure 1(b) shows the transmission spectra of this interleaver and illustrates the terminologies that are used in this paper. The free spectral range (*FSR*) in Fig. 1(b) refers to one period of the transmission spectrum. Within this FSR, the signals denoted as "1" and "2" in Fig. 1(a) are channeled to the bar port and to the cross port respectively. The channel crosstalk is an important figure of merit of an interleaver as it determines the effectiveness of the filter to suppress adjacent channels [18]. In this paper, we are optimizing the bandwidth for which the channel crosstalk is –20dB – the crosstalk of commercial telecom bandsplitter [19].

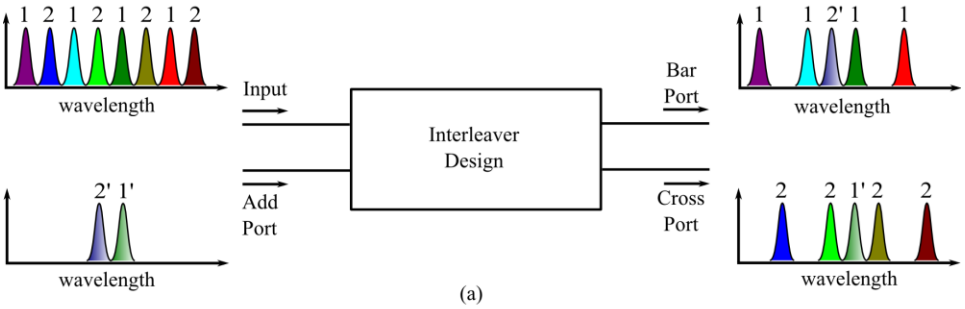

(a)

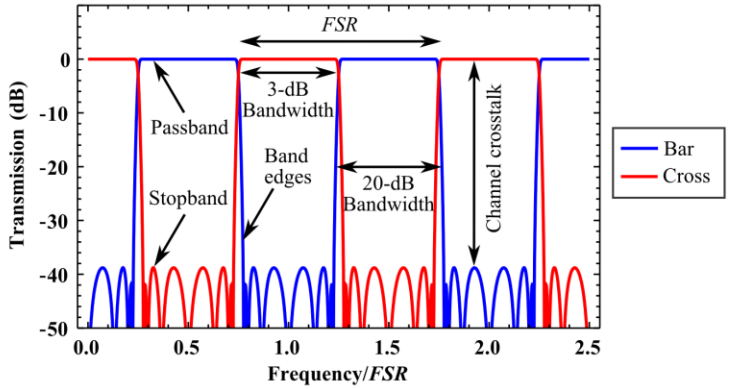

(b)

Fig. 1. Filtering function of an interleaver. (a) Multiplexing and demultiplexing of a comb of WDM signals. (b) Transmission spectra of the interleaver, illustrating the terminologies used in this paper.

Figure 2(a) shows a design of an interleaver based on an asymmetric MZI and a ring resonator first proposed by Oda et al [20]. The MZI consists of two 3-dB couplers and a path difference between the two arms. The length of the ring resonator (L_{ring}) is twice the length of the path difference and the *FSR* of the interleaver is determined by L_{ring}. The ring resonator is coupled to the shorter arm of the MZI with a coupling coefficient of κ_1. The transfer function of this single ring-assisted MZI interleaveris given by [21]:

$$H_{bar}(z) = \frac{1}{2}\left[\left(\frac{\rho_1 + z^{-2}}{1+\rho_1 z^{-2}}\right) - z^{-1}\right], \tag{1}$$

$$H_{cross}(z) = \frac{-j}{2}\left[\left(\frac{\rho_1 + z^{-2}}{1+\rho_1 z^{-2}}\right) + z^{-1}\right], \tag{2}$$

where $\rho_1 = (1-\kappa_1)^{0.5}$, $FSR = 2c / (n_g L_{ring})$, $z = \gamma \exp(j2\pi\nu)$, $\gamma = 10^{\alpha/20}$, α is the effective loss of the path difference or half the effective ring loss (in dB), $\nu = f / FSR = (n_g L_{ring}) / 2\lambda$ is the

frequency normalized to the *FSR*, c is the speed of light at vacuum, n_g is the group index of the device, and λ is the free space wavelength.

Considering a lossless device (α = 0), we show the performance of such a device for a coupling coefficient κ_1 of 0.89 (see Fig. 2(d) – blue dotted line). This value was obtained from Eq. (1) and (2) by optimizing the flatness of the passband response [21]. This device has a 20-dB bandwidth of 0.72 *FSR*. The slope of the band edges has a relatively slow roll-off and therefore the operating bandwidth of the device is low. It is essential to reduce the 20-dB bandwidth to as close as 0.5 *FSR* to fully utilize the entire operating spectrum. To further reduce the 20-dB bandwidth, we design higher order interleavers that have more ring resonators coupled to the arms of the MZI. When a second ring resonator is coupled to the longer arm of the MZI (see Fig. 2(b)), the device is shown to have a faster roll-off on the band edges [22]. Figure 2(d) (green dashed line) shows that the 20-dB bandwidth of this double ring-assisted MZI interleaver is reduced to 0.61 *FSR*. Another third ring resonator can be coupled to the shorter arm of the MZI to form the triple ring-assisted MZI interleaver (see Fig. 2(c)). This design further reduces the 20-dB bandwidth to 0.55 *FSR* (see Fig. 2(d) – red solid line). The transfer function of this triple ring-assisted MZI interleaver is given by:

$$H_{bar}(z) = \frac{1}{2}\left[\left(\frac{\rho_1 + z^{-2}}{1+\rho_1 z^{-2}}\right)\left(\frac{\rho_3 + z^{-2}}{1+\rho_3 z^{-2}}\right) - \left(\frac{\rho_2 + z^{-2}}{1+\rho_2 z^{-2}}\right) z^{-1}\right], \tag{3}$$

$$H_{cross}(z) = \frac{-j}{2}\left[\left(\frac{\rho_1 + z^{-2}}{1+\rho_1 z^{-2}}\right)\left(\frac{\rho_3 + z^{-2}}{1+\rho_3 z^{-2}}\right) + \left(\frac{\rho_2 + z^{-2}}{1+\rho_2 z^{-2}}\right) z^{-1}\right], \tag{4}$$

where $\rho_i = (1-\kappa_i)^{0.5}$, i = 1, 2, or 3, $FSR = 2c / (n_g L_{ring})$, $z = \gamma \exp(j2\pi\nu)$, $\gamma = 10^{\alpha/20}$, α is the effective loss of the path difference or half the effective ring loss (in dB), $\nu = f / FSR = (n_g L_{ring}) / 2\lambda$ is the frequency normalized to the *FSR*, c is the speed of light at vacuum, n_g is the group index of the device, and λ is the free space wavelength.

The addition of even more ring resonators to the MZI arms helps reduce the 20-dB bandwidth and therefore increase the operational bandwidth of the device. However, it also increases the attenuation of the transmitted signals due to the ring losses, as depicted by Eq. (3) and (4). Figure 3 illustrates the impact of ring loss on the cross port transmission spectra of an optimal triple ring-assisted MZI interleaver. In a lossless case (α = 0), the spectral response of the interleaver has a flat passband and fast roll-off on the band edges (see Fig. 3 – red solid line). The green dashed line and blue dotted line in Fig. 3 show that as the ring loss increases to 2 dB per ring and 4 dB per ring, the insertion loss of the interleaver increases. The passband also becomes not as flat and the roll-off on the band edges becomes less steep.

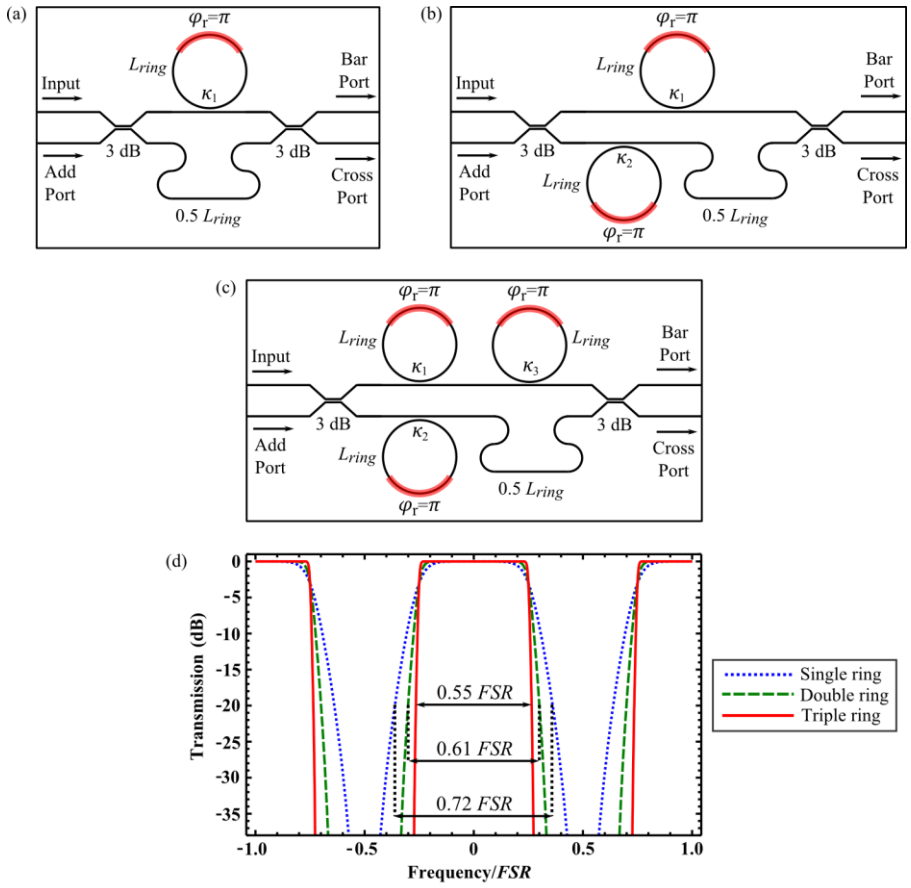

Fig. 2. Schematic of ring-assisted MZI interleavers. (a) Single ring-assisted MZI interleaver. (b) Double ring-assisted MZI interleaver. (c) Triple ring-assisted MZI interleaver. (d) Calculated cross port transmission spectra of an optimal single ring (κ_1 = 0.89), optimal double ring (κ_1 = 0.97, and κ_2 = 0.62), and optimal triple ring (κ_1 = 0.96, κ_2 = 0.68, and κ_3 = 0.25) assisted MZI interleaver.

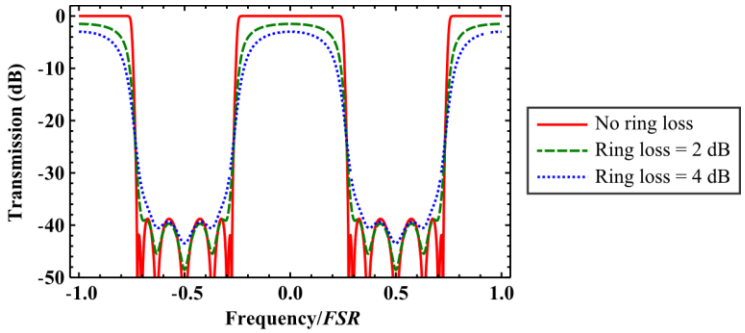

Fig. 3. Impact of ring loss on the cross port transmission spectra of an optimal triple ring-assisted MZI interleaver

The channel crosstalk of the triple ring-assisted MZI interleaver is highly dependent on the combination of the coupling coefficients κ_1, κ_2, and κ_3. Assuming that the waveguides are lossless in this device, we analyzed the effects of the coupling coefficients according to Eq. (3) and (4). Figure 4(a) shows the contour plot of the channel crosstalk of the interleaver as a

function of κ_1 and κ_2, with κ_3 optimized to be 0.25 for a passband bandwidth requirement of 0.55 *FSR*. In order to achieve a channel crosstalk of less than −20 dB in the device, we need to operate within the blue region in the contour plot. One can observe from Fig. 4(a) that the blue region occupies only a small area of the contour plot. This means that the values of κ_1 and κ_2 have to be controlled precisely. Figure 4(b) and 4(c) illustrate the high sensitivity of the device to small deviation of the coupling coefficient optimized values. Figure 4(b) shows the transmission spectra of the interleaver at the optimum operation (κ_1 = 0.96, κ_2 = 0.68, and κ_3 = 0.25, indicated by the white cross in the contour plot). The channel crosstalk increases from −40dB to −12 dB (see Fig. 4(c)) when the value of κ_1 changes from 0.96 to 0.8, indicated by the black cross.

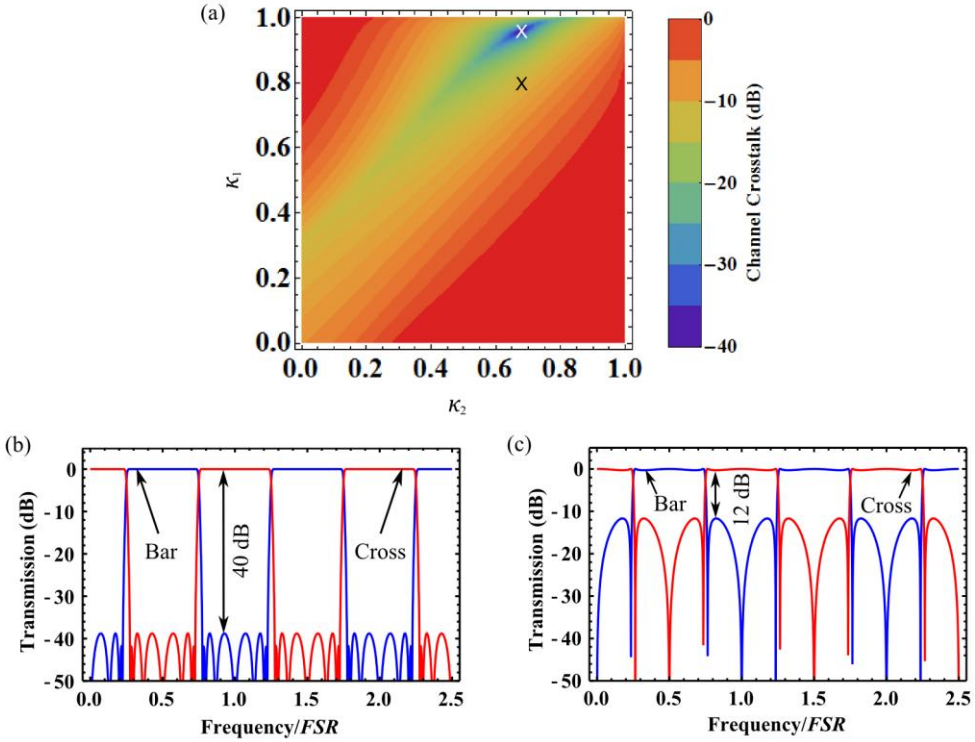

Fig. 4. Triple ring-assisted MZI interleaver. (a) Contour plot of the channel crosstalk as a function of κ_1 and κ_2, with the value of κ_3 optimized to be 0.25 for a passband bandwidth requirement of 0.55 *FSR*. (b) Simulated transmission spectra of the interleaver with κ_1 = 0.96 and κ_2 = 0.68, indicated by the white cross in the contour plot. (c) κ_1 = 0.8 and κ_2 = 0.68, indicated by the black cross.

In order to compensate for any fabrication imperfection, we design the device with full reconfiguration capability. To enable external control of each coupling coefficient independently, the waveguide-ring coupler is replaced with a thermo-optically tunable symmetric MZI coupler and the ring resonator with a racetrack resonator (see Fig. 5(a)) [23–26]. We do this modification to all the coupling regions, indicated by the blue regions in Fig. 5(b). The effective coupling of each MZI coupler can be externally controlled by changing the phase difference $\Delta\varphi = \varphi_1 - \varphi_2$ between the two arms of the MZI. The effective coupling is given by $K_{eff} = 4\kappa(1-\kappa)\cos^2(\Delta\varphi/2)$ where κ is the power coupling coefficient at each directional coupler of the MZI. The phase difference is controlled using the thermo-optic effect of silicon by placing a Nichrome (NiCr) heater on each arm of the MZI. To enable a full reconfiguration of K_{eff} from 0 to 1, the value of κ is set to be 0.5 (3 dB). A NiCr heater is also placed on each racetrack resonator and the asymmetric MZI path difference to tune the

effective phase of the device. The interleaver spectra can be shifted by one *FSR* by applying a π phase shift to the path difference between the asymmetric MZI arms for add/drop functionality. The merit of using thermal-optic tuning over carrier-induced tuning in this device is that it allows tuning over a larger range and the holding time is unlimited, whereas carrier-induced tuning is limited by thermal effects in the device. Additionally, in carrier-induced tuning, large amount of carrier injection into the silicon waveguides will result in a higher insertion loss of the device due to free carrier absorption [27].

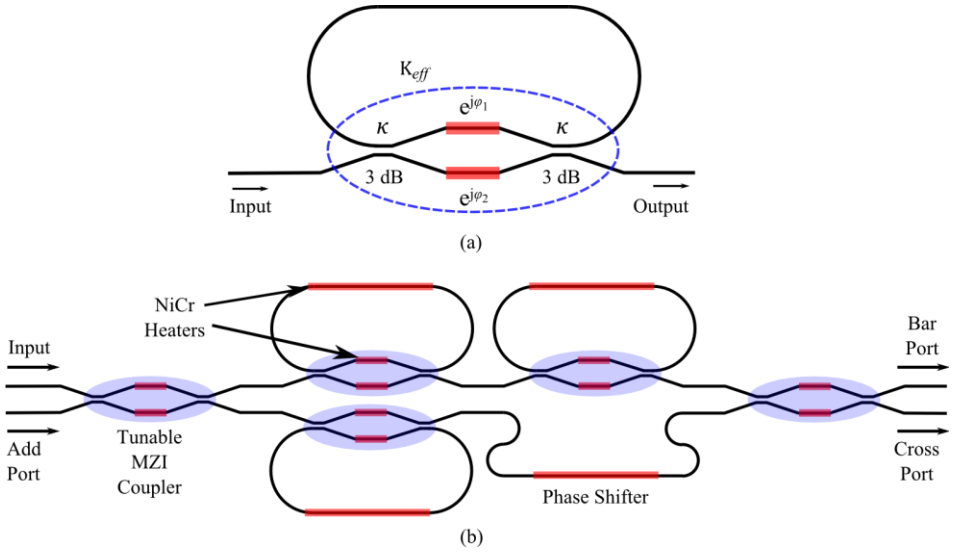

Fig. 5. Fully reconfigurable triple ring-assisted MZI interleaver. (a) Schematic of the tunable MZI coupler. (b) Fully reconfigurable triple ring-assisted MZI interleaver. All the blue coupling regions of the device are replaced with tunable MZI couplers. The rings are also replaced with racetrack resonators. A NiCr heater is placed on each arm of the MZI to tune the coupling by thermo-optic effect. A NiCr heater is also placed on each racetrack resonator and the asymmetric MZI path difference to tune the effective phase of the device.

3. Device fabrication

In this paper, the device is designed to have a *FSR* of 250 GHz by setting the length of the racetrack resonators (L_{ring}) to be 558 μm and the path difference between the MZI arms to be 279 μm. These values are calculated using the equation $FSR = 2c / (n_g L_{ring})$ by considering 450 nm x 250 nm channel waveguides with a group index of 4.3. We use a coupling gap of 200 nm and coupling length of 10 μm to realize the 3 dB directional couplers. We employ NiCr heaters at the MZI arms and racetrack resonators above the cladding to change the phase of each region independently. The NiCr heaters are 2 μm wide and 260 nm thick.

We fabricate the fully reconfigurable interleaver on a 250 nm SOI wafer with 3 μm of buried oxide using standard CMOS fabrication processes. First the 450 nm x 250 nm channel waveguides are patterned using e-beam lithography. The silicon waveguides are then etched using chlorine-based etcher. The e-beam resist is then stripped, and the etched structures are clad with 1 μm thick silicon oxide layer using plasma enhanced chemical vapor deposition to confine the optical mode. This 1 μm thick oxide cladding is sufficient to minimize the optical loss due to metal absorption [28]. 260 nm of NiCr are then evaporated on the MZI arms and racetrack resonators above the cladding to create the 2 μm wide heaters. Finally, 300 nm of gold (Au) are evaporated to define the electrode contacts using a lift-off process. The final fabricated device is illustrated in Fig. 6(a) and 6(b). The footprint of this triple ring-assisted MZI interleaver is 0.36 mm^2 without including the electrode contacts.

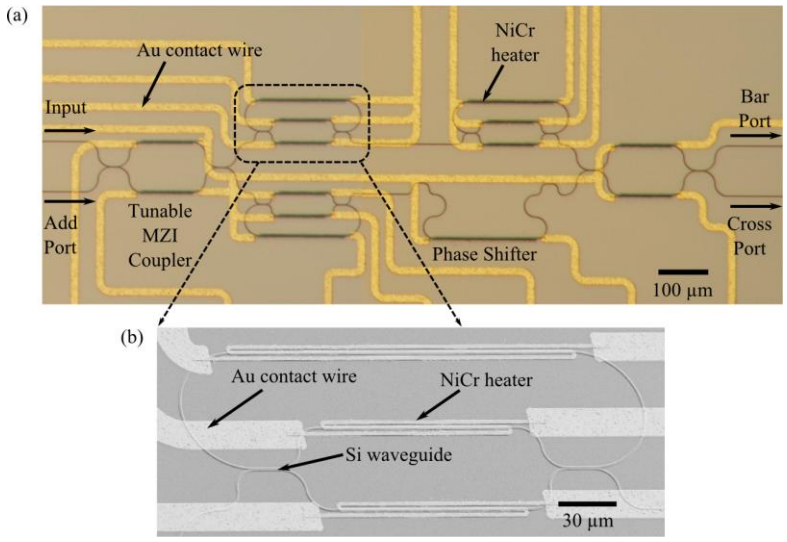

Fig. 6. Final fabricated device. (a) Optical microscope picture. (b) Scanning electron microscope (SEM) picture of the racetrack resonator coupled to the arm of the MZI.

4. Results and discussions

We demonstrate a 120 GHz 3-dB bandwidth interleaver with full reconfiguration capability. In order to characterize the device, we couple a tunable laser light source into the input port of the device through a polarization controller. The light output at the bar port and cross port are each collimated through a lens and collected at a photodetector to measure the transmission of TE polarized light (set by the polarization controller).

We thermally reconfigure the device to operate in the ideal coupling regime since the device performance is slightly suboptimal due to minor fabrication imperfections. Fine thermal-optic tuning is made to compensate for the fabrication imperfections. The total power consumption of this thermal reconfiguration is 5 mW. Figure 7(a) shows the transmission spectra of the device operating in the ideal coupling regime after thermal reconfiguration of the device. The total measured insertion loss from the fiber input to the output collected at the detector is 8 dB. It can be observed from the zoom-in spectra in Fig. 7(b) that the device is optimized to operate in the C-band. The transmission spectra of the bar and cross ports from 1548 nm to 1558 nm are clean and complementary. The device has a 3-dB bandwidth of 120 GHz and a flat passband over a 70 nm spectral range (from 1530 nm to 1600 nm). The transmission spectra also show a fast roll-off on the band edges with a 20-dB bandwidth of 142 GHz (equivalent to 0.57 *FSR*). The lowest channel crosstalk within this spectral range is measured to be −20 dB. This measured crosstalk of −20 dB is higher than the previously calculated crosstalk of −40 dB in Fig. 4(b) as it is assumed during the calculation that the waveguides are lossless and the power coupling coefficients of all the couplers are in the optimized values. The crosstalk, as observed in Fig. 7(a), is not −20 dB over the entire 70 nm spectral range. The crosstalk is as low as −20 dB at 1550 nm but increases to −10 dB at the lower bound of 1530 nm and −6 dB at the higher bound of 1600 nm. This varying performance of the device over the 70 nm spectral range is attributed to the wavelength sensitivity of the coupling coefficients. The performance of the device can be improved significantly by implementing a wavelength-insensitive 3 dB MZI coupler [29,30].

We also operate the device in the non-ideal coupling regime before any thermal reconfiguration so as to verify the dependence of the channel crosstalk on the coupling coefficients (κ_1, κ_2, and κ_3). Figure 8(a) shows that the transmission spectrum of the bar port does not complement the cross port. One can see from the zoom-in spectra in Fig. 8(b) that the channel crosstalk of the bar port is −5 dB and the crosstalk of the cross port is −10 dB.

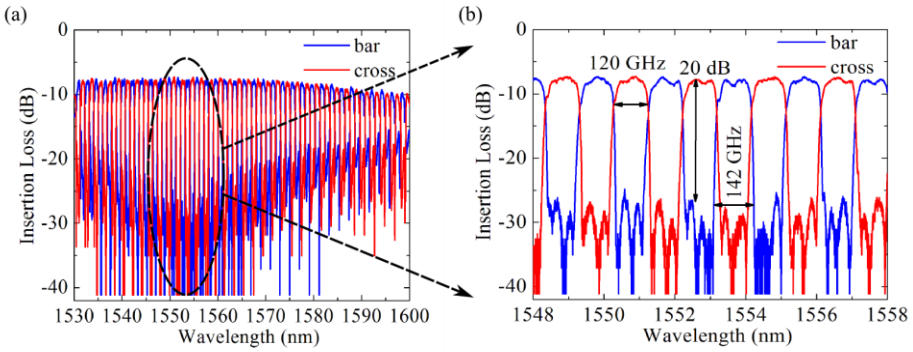

Fig. 7. Operation of the fabricated device in the ideal coupling regime. (a) Transmission spectra of the bar and cross port. (b) Zoom-in of the section in (a).

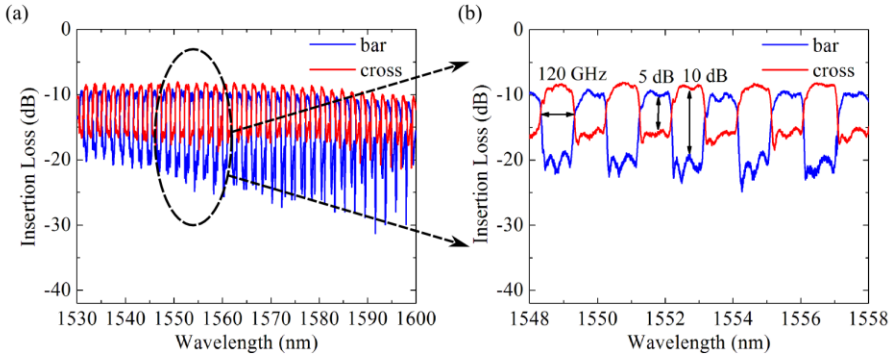

Fig. 8. Operation of the fabricated device in the non-ideal coupling regime. (a) Transmission spectra of the bar and cross port. (b) Zoom-in of the section in (a).

5. Conclusion

We have demonstrated a 120 GHz 3-dB bandwidth on-chip silicon photonic interleaver based on 3 ring resonators coupled to the arms of an asymmetric MZI. The fabricated device exhibits a flat passband over a broad spectral range of 70 nm (1530 – 1600 nm). The spectra show a rapid roll-off on the band edges with a 20-dB bandwidth of 142 GHz (equivalent to 0.57 *FSR*). The device is optimized for operation in the C-band with a channel crosstalk as low as –20 dB. This device also has full reconfiguration capability to compensate for fabrication imperfections. Integration of this interleaver with high-speed on-chip modulators and photodetectors in a WDM system is promising.

Acknowledgments

This work was partially funded by the DARPA MTO Si-PhASER Project Grant No. HR 0011-09-0013 with University of California, Davis. Lian-Wee Luo also acknowledges a fellowship from Agency of Science, Technology and Research (A*STAR), Singapore. This work was performed in part at the Cornell NanoScale Science and Technology Facility (CNF), a member of the National Nanotechnology Infrastructure Network, which is supported by the National Science Foundation. The authors would also like to thank H. Lira and G. Wiederhecker for helpful discussions.